JACS
JOURNAL OF THE AMERICAN CHEMICAL SOCIETY

ARTICLE

pubs.acs.org/JACS

Single Molecule and Single Atom Sensors for Atomic Resolution Imaging of Chemically Complex Surfaces

Georgy Kichin,[†,‡] Christian Weiss,[†,‡] Christian Wagner,[†,‡] F. Stefan Tautz,[†,‡] and Ruslan Temirov*[,†,‡]

[†]Peter Grünberg Institut (PGI-3), Forschungszentrum Jülich, 52425 Jülich, Germany

[‡]Jülich Aachen Research Alliance (JARA)-Fundamentals of Future Information Technology, 52425 Jülich, Germany

ABSTRACT: Individual Xe atoms as well as single CO and CH_4 molecules adsorbed at the tip apex of a scanning tunneling microscope (STM) function as microscopic force sensors that change the tunneling current in response to the forces acting from the surface. An STM equipped with any of these sensors is able to image the short-range Pauli repulsion and thus resolve the inner structure of large organic adsorbate molecules. Differences in the performance of the three studied sensors suggest that the sensor functionality can be tailored by tuning the interaction between the sensor particle and the STM tip.

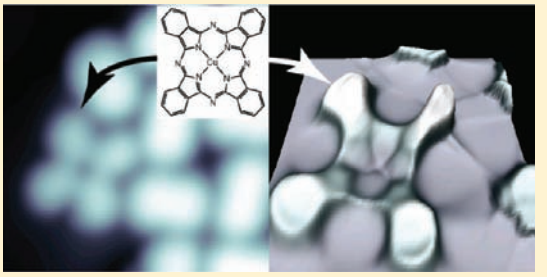

INTRODUCTION

Using force imaging with frequency modulated atomic force microscopy (AFM), it is possible to achieve atomic-scale image resolution on various surfaces[1,2] as well as resolve the inner structure of organic molecules.[3−5] The difficulties associated with high-resolution AFM stem from the necessity to reduce the influence of long-range forces on the macroscopic force sensors that are commonly employed.[1] In contrast, the scanning tunneling hydrogen microscopy (STHM) approach achieves atomic-scale resolution of molecular structures[6,7] and intermolecular interactions[8] with much less instrumental effort, relying simply on condensed molecular hydrogen or deuterium (H_2 or D_2) in the junction of a low-temperature scanning tunneling microscope (STM). To explain the STHM contrast, it has been proposed that a *single* H_2 or D_2 molecule in the tunneling junction acts as a *static* nanoscale force sensor and signal transducer: Interactions with the sample surface to be investigated change the position of the H_2 (D_2) molecule relative to the STM tip, thus varying the strength of Pauli repulsion between the tip and the H_2 (D_2); this is the "sensor" action.[7] The "transducing" effect is based on the coupling of the Pauli force to the tunneling conductance; the coupling occurs because an increasing repulsion between tip and sensor molecule progressively depletes the tip's density of states close to the Fermi level.[7]

Due to its small size, the STHM force sensor is intrinsically insensitive to long-range interactions. Hence, the difficulty associated with atomic-scale force imaging shifts toward sensor preparation. Fortunately, functional sensor structures form spontaneously when a small quantity of hydrogen or deuterium gas (less than one monolayer) is adsorbed in the STM junction at 5−15 K.[6] However, since neither H_2 nor D_2 can be imaged in the STM, the assumed structure of the nanoscale force sensor was up to now inferred from the properties of the STHM contrast itself, rather than determined independently. In these circumstances, an unambiguous proof for the idea that a *single* molecule acts as the force sensor has remained elusive. Here we overcome this ambiguity by demonstrating directly that a single atom or molecule that decorates the apex of an STM tip indeed produces an STHM-like resolution. Furthermore, the comparison between the imaging properties of various sensor molecules (xenon, carbon monoxide, and methane) reveals further properties of the STHM imaging mechanism.

EXPERIMENTAL SECTION

The imaging experiments reported here have been performed on a molecular monolayer film of 3,4,9,10-perylene-tetracarboxylic-dianhydride (PTCDA) adsorbed on Au(111). We used PTCDA/Au(111) in order to allow direct comparison to our previously reported data.[7,8] The STM tips were prepared from tungsten wire of 0.5 mm diameter by electrochemical etching. They were cleaned by electron bombardment in ultrahigh vacuum. Finally, the tip apex was covered with gold by numerous gentle indentations of the tip into the clean Au(111) surface. To achieve STHM-like resolution, the tip was further functionalized with one of the following three substances: xenon (Xe), carbon monoxide (CO), and methane (CH_4). Xe, CO, and CH_4 were deposited at 5 K by dosing the gases into the STM chamber through a shutter hole (diameter 0.5 cm) in the cryoshields that points directly toward the tunneling junction. For Xe and CO the surface coverage was less than 0.01 ML. In the case of CH_4 the coverage was less than 1 ML.

RESULTS AND DISCUSSION

We start our discussion of the experimental results with the case of Xe. After deposition, individual Xe atoms, which are observed in the STM as bright protrusions,[9−12] are predominantly found at the edges of PTCDA islands (cf. Figure 1a). As reported before, PTCDA forms two distinct monolayer structures on Au(111): the stable herringbone phase and the metastable

Received: May 20, 2011
Published: October 03, 2011

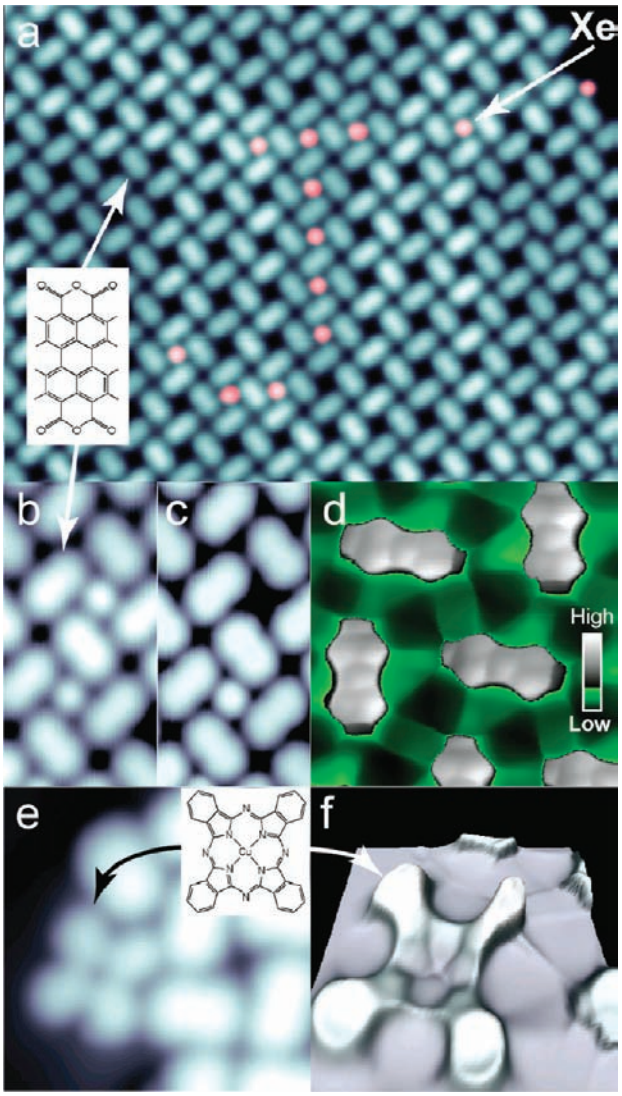

Figure 1. (a) 20 × 16 nm^2 constant current STM image of the letter J spelled with Xe atoms (false colored in pink) deposited in the voids of the square phase PTCDA island. The tunneling parameters: I = 55 pA, V = −10 mV. The chemical structure formula of PTCDA is shown in the inset. (b) Measured with the clean Au tip, constant current image of the 5 × 2.5 nm^2 area showing two Xe atoms residing in the PTCDA layer. The tunneling parameters are the same as in part a. (c) The same area as in part b scanned with the tip decorated with a single Xe atom picked up from the upper slot shown in part b. Tunneling parameters as in part a. (d) 2.5 × 2.5 nm^2 constant height image of the herringbone ordered PTCDA domain recorded with the Xe decorated tip. The tip is stabilized above the center of PTCDA at I = 50 pA, V = −10 mV and then moved by 2.5 Å closer to the surface. The image is taken at the bias V = −10 mV. The color palette is shown in the inset. Brightness scale: I_{low} = −0.4 nA, I_{high} = −8 nA. (e) A single CuPc molecule attached to the edge of the PTCDA/Au(111) island. Tunneling parameters I = 55 pA, V = 100 mV. The chemical structure formula of CuPc is shown in the inset. (f) A constant height image of the CuPC molecule from part e, measured with the Xe tip. The tip is stabilized at I = 55 pA, V = 10 mV over the clean Au surface and then shifted by 0.8 Å closer to the surface. The image is taken at the bias V = 10 mV. Brightness scale: I_{low} = 0.03 nA, I_{high} = 6.5 nA. The 3D representation was used for a full visualization of the wide dynamic range of the experimental contrast. All of the images were prepared using WSxM software.[13].

square phase.[8] Following the recipe of Eigler et al.,[11,12] we picked up individual Xe atoms, one at a time, with the STM tip and deposited them into the voids of the square-phase islands, one atom per void (cf. Figure 1a−c). Once deposited, the Xe atoms can be stored in the voids at 5 K for unlimited time, or picked up again by the tip. We found the Xe atom manipulation protocol to be very reproducible. This has allowed us to study the imaging properties of STM tips decorated with a *single* Xe atom systematically.

When scanned at ordinary tunneling conditions, Xe-decorated tips ("Xe-tips") yield a slight enhancement of spatial image resolution (compare parts b and c of Figure 1), in agreement with results reported by Yazdani et al.[12] However, when Xe-tips are moved closer to the surface, they develop a new type of contrast (cf. Figure 1d). Comparing Figure 1d to Figure 1c from ref 8, we see that the contrast generated by the Xe-tip is almost identical to the STHM contrast obtained with D_2. Thus, the experiments with Xe allow significant progress in our understanding of STHM: Because the structure of the Xe-tip is known, it becomes unambiguously clear that the STHM-type contrast is produced by a *single particle* (Xe or D_2) which is bound to the apex of an STM tip, from where it interacts with the sample and thus senses the force exerted on it by the surface. A comparison between D_2-sensors and Xe-sensors shows that the mass of the involved particle has limited (if any) influence on the image contrast obtained. Therefore, also the *static* model of the STHM force sensor that was proposed in our earlier work is confirmed.[7] From now on, we will refer to STHM-like contrast simply as STHM contrast, regardless of the employed sensor molecule.

Methodologically, the employment of Xe has advantages: First, the preparation of Xe-sensors as described above, for which a very small coverage of Xe on the surface is sufficient, is more straightforward and controlled than the preparation of H_2- or D_2-sensors (ref 7). Second, Xe-sensors exhibit an improved mechanical stability during scanning, which helps to extend the applicability of STHM. As an example, we have imaged a copper phthalocyanine (CuPc) molecule attached to the edge of a molecular PTCDA island. In the imaged area the surface has a lower degree of local order and thus interacts more strongly with the tip, thereby taxing its mechanical stability (cf. Figure 1e,f). Nevertheless, the Xe-sensor successfully resolves the structure of the CuPc molecule, thus demonstrating that more complex organic structures than fused aromatic carbon rings can be imaged.

As the stability of any single particle sensor at the apex of an STM tip is determined by the particle's interaction with the tip, our Xe experiments open a new perspective for tailoring the sensor properties via tuning the tip−particle interaction strength. To explore this possibility, we have additionally tested sensors fabricated from single carbon monoxide (CO) and methane (CH_4) molecules.

Similar to Xe, CO can be attached to the STM tip in a controlled and reproducible manner.[3,14] This can be seen in Figure 2a,b: After Figure 2a had been recorded, the CO molecule in the upper part of Figure 2a was picked up with the STM tip by positioning the tip over it at I = 50 pA, V = −10 mV and applying the bias of 2 V. If the same sample area is scanned with the CO-modified tip (Figure 2b), the CO molecule in the lower part of the image is rendered as a white spot in a dark ring.[14] All CO-terminated tips formed in this way were able to resolve the inner structure of PTCDA (cf. Figure 2c). At the same time we found characteristic differences between the images recorded with the Xe- and CO-sensors, respectively: On one hand, the CO-sensor yields better resolution of the aromatic backbone of PTCDA (with the exception of the two C_5O heterorings located at the

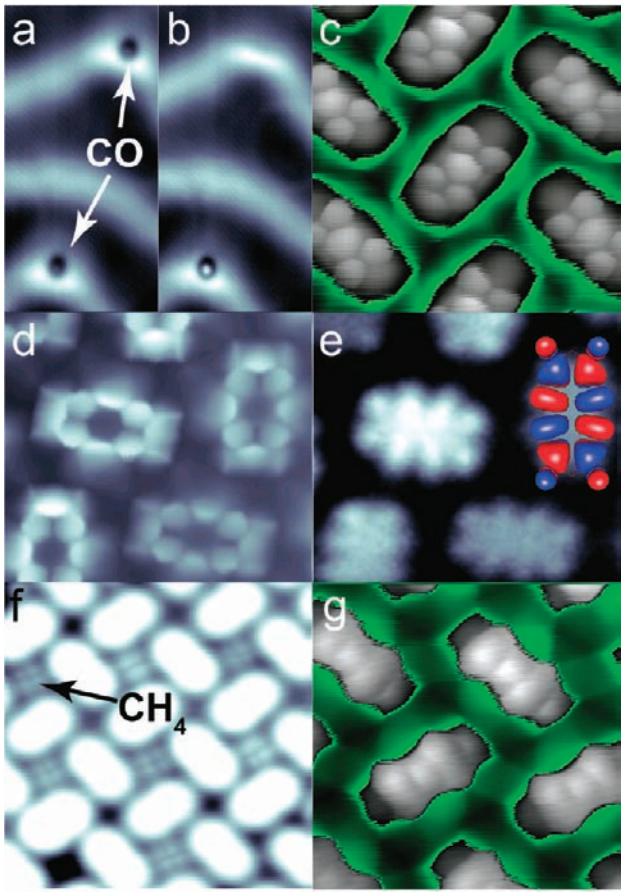

Figure 2. (a) 5 × 10 nm^2 constant current STM image of the Au(111) surface with the two adsorbed CO molecules. (b) The same as part a but made after picking up the upper CO molecule with the tip. (c) 2.5 × 2.5 nm^2 constant height image of the herringbone ordered PTCDA domain, recorded with CO. The tip is stabilized above the center of PTCDA at I = 50 pA, V = −10 mV and then moved by 1.4 Å closer to the surface. The color palette as in Figure 1d with the following brightness scale: I_{low} = −80 pA, I_{high} = −0.7 nA. (d) dI/dV image recorded with CO. The tip stabilization is the same as in part c. The image was recorded using the lock-in technique with the following parameters: f_{mod} = 37.77 kHz, V_{mod} = 20 mV, V_{bias} = −1.6 V. (e) dI/dV image recorded with the clean Au tip. The tip stabilization is the same as in part d. The image was recorded using the lock-in technique with the same parameters as in part d, but V_{bias} = −1.7 V. The calculated image of the PTCDA HOMO is overlaid in the upper right corner for comparison with the experimental dI/dV contrast. (f) 5 × 5 nm^2 constant current STM images of the PTCDA/Au(111) surface with CH_4 molecules adsorbed in the voids of the square phase domain. Tunneling parameters: I = 250 pA, V = −10 mV. (g) 2.5 × 2.5 nm^2 constant height image of the herringbone ordered PTCDA domain, recorded with the CH_4 decorated tip. The tip is stabilized above the center of PTCDA at I = 50 pA, V = −10 mV and then moved by 2.7 Å closer to the surface. The color palette as in Figure 1d with the following brightness scale: I_{low} = −0.4 nA, I_{high} = −6.5 nA.

ends of the molecule). On the other hand, the CO-induced contrast in the spaces between the molecules, where Xe-, H_2-, and D_2-sensors record an image pattern that is related to the intermolecular hydrogen-bond network,[8] is much weaker than for the other sensor particles.

CO-sensors are characterized by an exceptional stability with respect to large bias voltages that are applied to the junction. This is demonstrated by the image of PTCDA/Au(111) in Figure 2d, which was recorded with the CO-sensor at −1.6 V applied to the sample. If this STHM image is compared to Figure 2e, a conventional local density of states (LDOS) image of the PTCDA HOMO (HOMO = highest occupied molecular orbital), measured with a clean metal tip at the same tunneling conditions as Figure 2d, it becomes apparent once more that the STHM contrast is *not* a mere enhancement of the conventional LDOS resolution that derives from molecular electronic resonances. However, it is also true that the STHM contrast is affected by the sample LDOS, in agreement with the model of the sensor proposed earlier.[7] In Figure 2d this influence of the LDOS makes the central ring appear dark, because the HOMO has a node there.

The third type of sensor that we investigated here is made with a single CH_4 molecule. In contrast to Xe- and CO-sensors, CH_4-sensors have to be prepared differently: Although individual CH_4 molecules can be imaged with conventional STM in the voids of the square phase of PTCDA/Au(111) where they spontaneously adsorb during the deposition (cf. Figure 2f), single CH_4 molecules cannot be picked up reproducibly from these voids with the STM tip. Therefore, larger quantities of CH_4 have to be adsorbed on the surface; the sensor is then created by spontaneous adsorption of a CH_4 molecule at the tip apex, where its adsorption is additionally stabilized by the further CH_4 molecules present in the vicinity. The preparation procedure of the CH_4 sensor is thus very similar to the recipe used for obtaining STHM junctions with H_2 or D_2.[6]

Figure 2g reveals that CH_4-sensors also produce STHM resolution. To compare the contrasts obtained with different types of sensors, we plot in Figure 3a conductance profiles measured at constant height along two different lines above the PTCDA/Au(111) surface: The profiles in the left panel of Figure 3a are recorded above the aromatic rings of the PTCDA molecule, while the profiles on the right are measured above the area where intermolecular hydrogen bonds are located (cf. insets in the right and left panels of Figure 3a). The profiles recorded above the PTCDA molecule exhibit the corrugation of the "Pauli repulsion contrast" that is described in ref 7. The figure shows that the images recorded with the Xe- and CH_4-sensors are laterally distorted: in both cases, the three aromatic rings along the profile appear to have different sizes. Also, Xe- and CH_4-sensors yield an asymmetric contrast within each ring. Since the position of the imaged PTCDA molecule does not change during the scan, the observed image distortions must be caused by deformations of the tip−sensor complex that occur as the tip is scanned along the line. Notably, the contrast generated by the CO-sensor is less distorted and more symmetric. This property of the CO-sensor may be rationalized by the stronger bonding of CO to the gold tip, as compared to Xe and CH_4.[15,16]

Looking at the signal above the hydrogen bonds (cf. Figure 3a, right panel), we notice that the imaging performance is reversed: Here, the Xe- and CH_4-sensors provide a higher sensitivity than the CO-sensor. Because the mechanism of hydrogen bond imaging in STHM is not yet fully understood, it should be very helpful to relate the poor performance of the CO-sensor in this respect to its distinctive properties; this may provide a crucial hint about the mechanism with which hydrogen bonds are imaged.

Why does the CO-sensor perform worse in resolving the hydrogen bond network? To address this question, we analyze conductance versus distance spectra $G(z)$ that are measured while the tip with the attached sensor molecule approaches the surface (cf. Figure 3b). All $G(z)$ curves plotted in Figure 3b

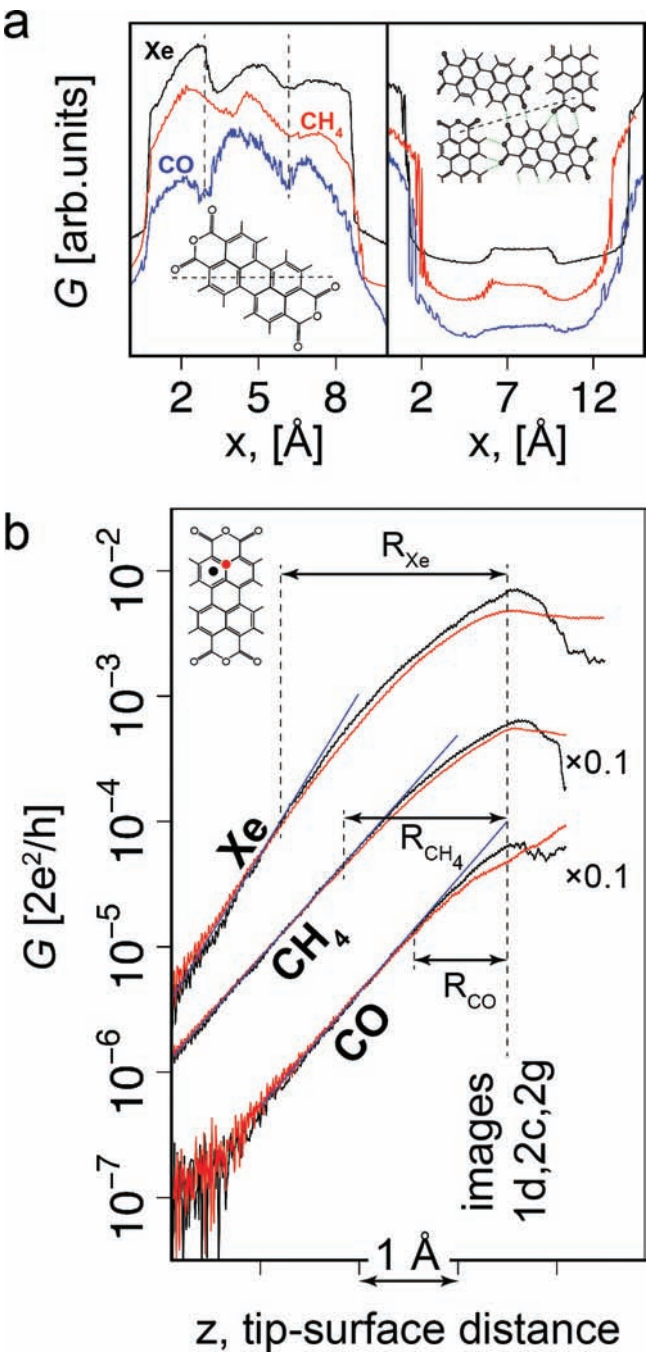

Figure 3. (a) Conductance line profiles measured along the path marked by the dashed lines in the respective insets. The black curve was extracted from Figure 1d measured with Xe, the red curve from Figure 2g measured with CH_4, and the blue curve from Figure 2c measured with CO. To facilitate the comparison between the profiles, each of the curves was divided by the factor $|G_{max} - G_{min}|$, where G_{max} (G_{min}) are the maximum (minimum) values of the conductance in the treated curve. The resulting curves were additionally shifted along the vertical axis. (b) The approach conductance spectra of the Xe, CO, and CH_4 sensors measured from the stabilization point: $I = 50$ pA, $V = -10$ mV. Horizontal axis shows the relative distance between the surface and the tip. The curves were shifted along the z-axis such that the tip−surface distances, at which the Figures 1d, 2c, and 2g were scanned, coincide. For clarity the curves of CH_4 and CO were multiplied by 0.1.

exhibit a pronounced nonexponential behavior at small tip−sample distances. In ref 7 we have used the analogous behavior of H_2 or D_2 junctions to demonstrate how the force signal from the sample surface couples to the junction conductance, namely via the depletion of the tip DOS by Pauli repulsion between the tip and the D_2 molecule adsorbed at the apex.[7] In ref 7 we concluded that this mechanism, which we have termed the "transducer action", is the key element of the STHM imaging process. Figure 3b confirms that the Xe-, CH_4-, and CO-sensors act as transducers in the very same way that H_2 and D_2 do, and therefore are indeed expected to provide an STHM-like image resolution. In fact, recording $G(z)$ spectra above a carbon atom (red curve) and a C_6 ring (black curve) of the PTCDA backbone, we can directly observe that both conductance curves start to deviate from each other more and more as the tip approaches the surface. The appearance of this deviation marks the onset of the STHM image corrugation. Our experiments show that each sensor molecule indeed achieves its optimal resolution of the carbon backbone (shown in images in Figures 1d, 2c, and 2g, respectively) at a distance where the difference between the red and the black $G(z)$ spectra is pronounced.

Although all three sensors transduce force into conductance (as suggested by the nonexponential $G(z)$ curves, see above), they do it in a slightly different manner. To facilitate the comparison between the sensors, we have aligned all $G(z)$ curves at the respective tip−surface distances where optimal image contrast is obtained. It is apparent that the tip−surface distance range in which the sensors are sensitive to any influence whatsoever from the sample surface (and thus produce a measurable signal) differs substantially between the three sensor particles. This range can be quantified by the parameter R which is defined as the difference between the distance at optimal contrast and the distance at which the particular $G(z)$ curve starts to deviate form exponential growth. Note that the value of R is determined by the interaction of the sensor with the tip and the surface and should not be merely associated with the size of the sensor molecule. According to Figure 3b, the values R_{Xe} and R_{CH4} are noticeably larger than R_{CO}, which means that the Xe- and CH_4-sensors produce detectable output in a wider range of tip−surface distances, while the sensitivity of the CO-sensor decays faster as the tip is moved away from the sample surface.

To summarize our discussion of the CO-sensor, we have seen (i) that the CO-sensor has a substantially shorter sensitivity range than Xe- and CH_4-sensors (Figure 3b) and (ii) that it yields the poorest hydrogen bond contrast (Figure 2c). We suggest that this is not a mere coincidence, but that the shorter-range sensitivity of the CO-sensor is indeed the reason for its poor hydrogen bond resolution. This suggestion is based on the fact that, in the area between the molecules where the hydrogen bond network is located, the effective tip−surface distance is larger than on top of PTCDA (we note again that all STHM images reported in this paper have been measured in constant height mode); because of their short-range sensitivity, the increased tip−surface distance above the interstitial areas must affect the performance of CO-sensors in a more pronounced way than of the Xe- and CH_4-sensors.

The coincidence between the hydrogen bond imaging performance of the CO-sensor and its short-range sensitivity allows us to infer that the interaction at the origin of the hydrogen bond contrast in STHM is longer-range and thus not related to the short-range Pauli repulsion which generates the contrast above the molecules. This conjecture is fully consistent with the model of the STHM sensor as proposed in ref 7, because the model separates the sensing and transducing functions of the sensor particle: Although the signal transduction always arises because

of Pauli repulsion between the tip and the sensor particle at the apex, this transduction will convert any type of force signal from the surface that acts on the sensor particle. Following this model, the images of the PTCDA/Au(111) in Figures 1d and 2g show that the Xe atom and the CH_4 molecule at the apex of the STM tip experience two types of interactions: the Pauli repulsion above PTCDA molecules and another, longer-range interaction above the hydrogen bonds.

CONCLUSIONS

In conclusion, we have directly demonstrated that individual Xe atoms as well as single CH_4 or CO molecules attached to the tip of a STM act as nanoscale force sensors, transducing force signals from the sample surface into variations of the junction conductance. As a result, these sensors can be used to image short-range forces. All three sensors successfully resolve the inner structure of large organic molecules by imaging the short-range Pauli repulsion. We found that CO produces the strongest Pauli repulsion contrast of the three. This contrast is of similar quality as the Pauli repulsion contrast due to hydrogen or deuterium. In addition, CO yields images of least distortion, probably because of its more rigid bond to the metal tip. In conductance versus distance spectroscopy, we have found that the distance range in which the three sensors produce a measurable output is the shortest for CO. The limited-range sensitivity explains the failure of CO-sensors to resolve the hydrogen bond network in PTCDA layers. At the same time, it suggests that the hydrogen bond contrast is not due to Pauli repulsion, but stems from another, longer-range interaction. Altogether our data show that the STHM method belongs to a wider family of *atomic-sensor microscopy* techniques, in which an individual atom, molecule, or possibly a larger particle attached to the tip of a scanning probe microscope interacts with the imaged surface and simultaneously converts its interaction into a signal detectable within the particular scanning probe approach.

AUTHOR INFORMATION

Corresponding Author
r.temirov@fz-juelich.de

ACKNOWLEDGMENT

We thank M. Sokolowski (Bonn) for helpful discussions. R.T. acknowledges support by the Helmholtz-Gemeinschaft.

REFERENCES

(1) Giessibl, F. J. *Rev. Mod. Phys.* **2003**, *75*, 949–983.
(2) Sugimoto, Y.; Pou, P.; Abe, M.; Jelinek, P.; Perez, R.; Morita, S.; Custance, O. *Nature* **2007**, *446*, 64–67.
(3) Gross, L.; Mohn, F.; Moll, N.; Liljeroth, P.; Meyer, G. *Science* **2009**, *325*, 1110–1114.
(4) Gross, L.; Mohn, F.; Moll, N.; Meyer, G.; Ebel, R.; Abdel-Mageed, W. M.; Jaspars, M. *Nat. Chem.* **2010**, *2*, 821–825.
(5) Gross, L. *Nat. Chem.* **2011**, *3*, 273–278.
(6) Temirov, R.; Soubatch, S.; Neucheva, O.; Lassise, A. C.; Tautz, F. S. *New J. Phys.* **2008**, *10*, 053012.
(7) Weiss, C.; Wagner, C.; Kleimann, C.; Rohlfing, M.; Tautz, F. S.; Temirov, R. *Phys. Rev. Lett.* **2010**, *105*, 086103.
(8) Weiss, C.; Wagner, C.; Temirov, R.; Tautz, F. S. *J. Am. Chem. Soc.* **2010**, *132*, 11864–11865.
(9) Eigler, D. M.; Schweizer, E. K. *Nature* **1990**, *344*, 524–526.
(10) Eigler, D. M.; Weiss, P. S.; Schweizer, E. K.; Lang, N. D. *Phys. Rev. Lett.* **1991**, *66*, 1189–1192.
(11) Eigler, D. M.; Lutz, C. P.; Rudge, W. E. *Nature* **1991**, *352*, 600–603.
(12) Yazdani, A.; Eigler, D. M.; Lang, N. D. *Science* **1996**, *272*, 1921–1924.
(13) Horcas, I.; Fernandez, R.; Gomez-Rodriguez, J. M.; Colchero, J.; Gomez-Herrero, J.; Baro, A. M. *Rev. Sci. Instrum.* **2007**, *78*, 013705(8).
(14) Bartels, L.; Meyer, G.; Rieder, K. H. *Appl. Phys. Lett.* **1997**, *71*, 213–215.
(15) Gottfried, J. M.; Schmidt, K. J.; Schroeder, S. L. M.; Christmann, K. *Surf. Sci.* **2003**, *536*, 206–224.
(16) Bruce, L. A.; Sheridan, M. H. *J. Chem. Soc., Faraday Trans.* **1972**, *68*, 997–1009.